CHAPTER 8. STOCHASTIC FORMATION MISSION DESIGN PROBLEM

In this chapter, to show the effectiveness of the methodology described in Chapter 6, in solving the formation mission design problem in the presence of uncertainties, the results of two different numerical experiments will be described. All the experiments involve transoceanic eastbound flights operated by Airbus 330-200. In the first experiment, a three-aircraft formation mission design problem is solved, in which uncertainty regarding fuel burn savings is considered. In the second experiment, a two-aircraft formation mission design problem is solved, in which uncertainty regarding departure times of the aircraft is considered. For each experiment, a detailed description of the results is given along with a comparison with the results obtained in the absence of uncertainties and in solo flights. Finally, a sensitivity analysis of the stochastic solutions of the second experiment has been conducted.

8.1. General description of the experiments

The following numerical experiments have been carried out:

- Experiment A: Three-aircraft transoceanic mission design with uncertainty in the fuel burn savings.

- Experiment B: Two-aircraft transoceanic mission design with uncertainty in departure times of the flights.

Both experiments involve transoceanic eastbound flights. Wind data from the ERA-Interim reanalysis database of the ECMWF are used. As mentioned in Chapter 3, in this thesis only the cruise phase has been considered; the rest of the flight phases are neglected. Thus, the initial and final locations of the cruise phase of the flights are assumed to be the latitudes and longitudes of the departure and arrival airports of each flight at cruise altitude. Airbus A330-200 aircraft BADA models are considered for each flight. The initial masses of the aircraft are assigned, as are the initial and final velocities, which are set at typical cruise values for the selected aircraft models. The initial heading angles are set to the initial heading angles of the orthodromic paths between the initial and final locations of each flight. The time and fuel burn weighting parameters, α_t and α_f, in the objective functional (3.18) are set to 0.3 and 0.7, respectively, based on the CI definition, as explained in Section 3.4.

The numerical experiments have been conducted on a 3.6 GHz Intel Core i9 computer with 32 GB RAM. The computational times reported in the following sections include both the time required to generate the warm-start solution and the time to find the optimal solution of the problem. The warm-start solution is a feasible solution of the problem generated by the NLP solver from an initial guess of the solution. Several initial guesses have been tried to obtain the warm-started solution in order to ensure that the global optimum is reached. Initial guesses for the latitude, the longitude, and the heading angle are generated using the orthodromic paths between the departure and arrival locations of each flight. Typical cruise velocity and fuel consumption of the aircraft model selected are used to generate the initial guesses of the velocity and the mass of each aircraft during the flight, respectively.

8.2. Experiment A: Three-aircraft transoceanic mission design with uncertainty in the fuel burn savings

8.2.1. Description of the experiment

Experiment A involves three transoceanic eastbound flights, Flight 1, Flight 2, and Flight 3, with uncertainty in the fuel burn savings for the trailing aircraft. The three flights considered in this experiment have the following departure and arrival locations:

- Flight 1: New York (JFK) - Paris (CDG).
- Flight 2: Boston (BOS) - Madrid (MAD).
- Flight 3: Montreal (YUL) - London (LHR).

The departure times of Flight 1, Flight 2, and Flight 3 are set to 10:15, 10:30, and 10:50, respectively. The boundary conditions for the state variables of the three aircraft are given in Table 8.1. Flight 1, Flight 2, and Flight 3 are operated by Aircraft 1, Aircraft 2, and Aircraft 3, respectively.

The relative position of each aircraft in the formation is selected in advance. In case of two-aircraft formation flights that include Aircraft 2, Aircraft 2 will be the leader aircraft and Aircraft 1 or Aircraft 3 will be the trailing. In case of two-aircraft formation flights that do not include Aircraft 2, Aircraft 3 will be the leader aircraft and Aircraft 1 will be the trailing. In case of three-aircraft formation flights, Aircraft 2 will be the leader aircraft, Aircraft 3 the intermediate, and Aircraft 1 the trailing.

Table 8.1. Experiment A: Boundary conditions of the three flights.

Symbol	Units	Flight 1	Flight 2	Flight 3
ϕ_I	[deg]	40.64	42.36	45.47
ϕ_F	[deg]	48.85	40.48	51.47
λ_I	[deg]	−73.78	−71.06	−73.74
λ_F	[deg]	2.35	−3.57	−0.12
χ_I	[deg]	+54.26	69.25	+55.53
V_I	[m/s]	240	240	240
V_F	[m/s]	220	220	220
m_I	[kg]	215 000	210 000	220 000

The random variable that represents the fuel burn savings for the trailing aircraft is denoted by θ. This random variable is modeled as a Gaussian random variable with mean 0.1 and standard deviation 0.02, i.e., $\theta \sim N(0.1, 0.02)$, based on several aerodynamic models and flight tests reported in [Kent and Richards, 2021]. The departure times are fixed.

Solving this problem entails deciding which mode of flight, i.e., formation or solo flight, is optimal, the expected values and standard deviations of the latitude and longitude of the optimal trajectories of each aircraft as functions of time, and the expected values and standard deviation of the timing of the trajectory as functions of the orthodromic distance from the departure locations. They include the expected values and the standard deviations of the arrival times and, in the case of formation flight, the expected values and the standard deviations of the latitude, longitude, and time of the rendezvous and splitting locations.

8.2.2. Results

The sequence of discrete states obtained in the solution is the following:

- State 1: All the aircraft fly solo.
- State 2: Aircraft 1 and Aircraft 2 fly in a two-aircraft formation and Aircraft 3 flies solo.
- State 3: All the aircraft fly in a three-aircraft formation.
- State 4: Aircraft 1 and Aircraft 3 fly in a two-aircraft formation and Aircraft 2 flies solo.
- State 5: All the aircraft fly solo.

Optimal routes

The expected values of the longitude and latitude of the optimal routes obtained in the solution together with the corresponding 95% confidence envelopes are represented on the relevant map together with the wind field in Fig. 8.1 and as functions of time in Fig. 8.2.(a) and Fig. 8.2.(b), respectively.

Fig. 8.1. Experiment A: Expected values of the latitude and longitude of the optimal trajectories of each aircraft together with the corresponding 95% confidence envelopes represented on the relevant map together with the wind field.

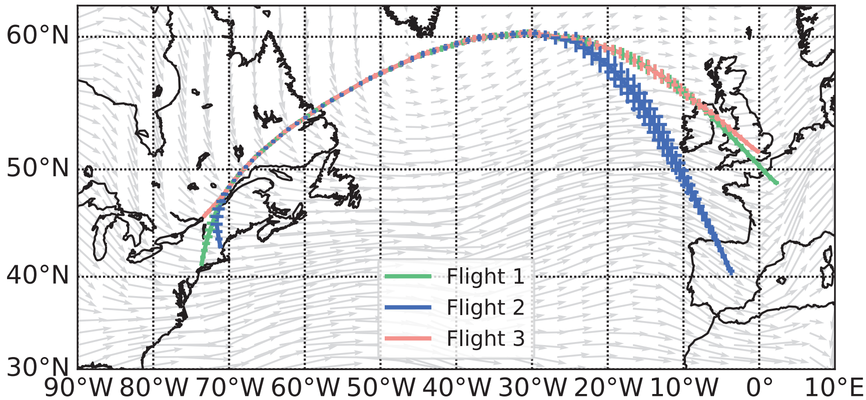

Optimal state and control variables

The expected values of the rest of the state variables, namely, the mass, the heading angle, and the Mach number, together with the corresponding 95% confidence envelopes are represented as functions of time in Fig. 8.2.(c), Fig. 8.2.(d), and Fig. 8.2.(e), respectively. The expected values of the control variables are represented for the three flights in Fig. 8.3. Green, blue, and red lines correspond to Flight 1, Flight 2, and Flight 3, respectively. For a better understanding of these figures, the portions of the plots of the variables that correspond to formation flight are represented on a gray background. In particular, the portions of the plots that correspond to State 2 and State 4, which includes a two-aircraft formation, are represented on a light gray background, whereas the portion of the plots that correspond to State 3, which includes a three-aircraft formation, is represented on a dark gray background.

It is important to note that all the optimal solutions obtained considering the fuel burn savings that correspond to the nodes of the gPC expansion of the random variable $\theta \sim N(0.1, 0.02)$ are formation missions with the same structure.

The control variables vary in a quite smooth way.

Optimal rendezvous and splitting times

The expected values of the rendezvous and splitting times are reported in Table 8.2 together with the corresponding 95% confidence interval. State 2, in which Aircraft 1 and Aircraft 2 fly in formation and Aircraft 3 flies solo, has the shortest duration.

Fig. 8.2. Experiment A: Expected values of the state variables of the optimal trajectories of each aircraft together with the corresponding 95% confidence envelopes.

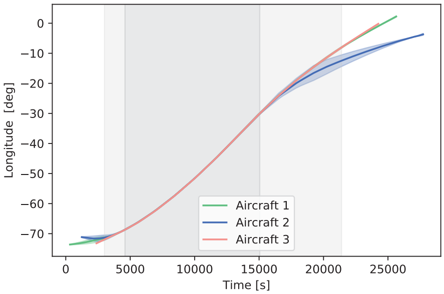

(a) Longitude

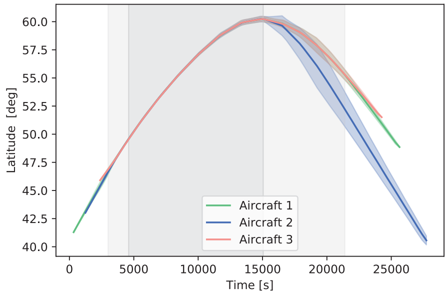

(b) Latitude

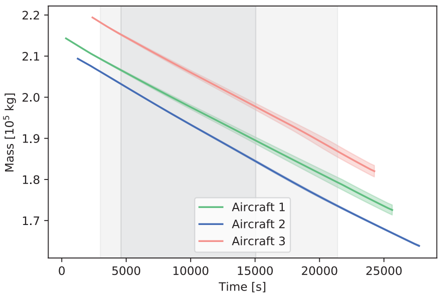

(c) Mass

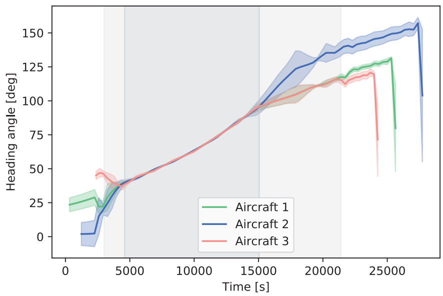

(d) Heading angle

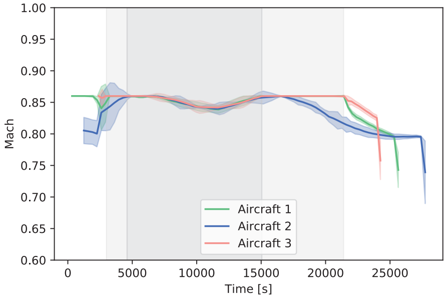

(e) Mach number

Fig. 8.3. Experiment A: Expected values of the control variables of each aircraft.

(a) Lift coefficient

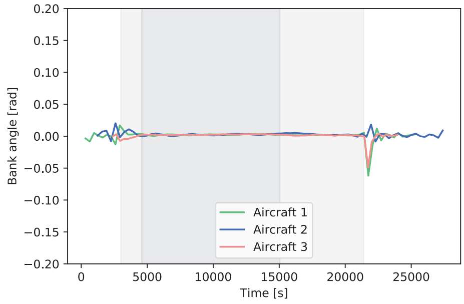

(b) Bank angle

(c) Adimensional thrust

Spatial variability

Regarding the spatial variability of the solution, it can be observed in Fig. 8.1, Fig. 8.2.(a), and Fig. 8.2.(b), that both geographical coordinates have a similar behavior. In the first two discrete states, the spatial variability is rather low, and in State 3, it is almost negligible. Then, near the first splitting location, the spatial variability starts increasing for all the flights. Finally, it decreases when the aircraft are approaching the final locations. Hence, the second splitting location has a significant dependency on the random variable θ and, consequently, both the duration and the traveled distance in State 3 have a significant dependency on it. Flight 2 has the greatest spatial variability.

Temporal variability

In addition to the spatial variability, the temporal variability is also quantified in order to have complete information regarding the spatio-temporal variability of the solution. The expected values of the timing of the solution together with the corresponding 95% confidence envelopes are represented in Fig. 8.4 as functions of the orthodromic distance from the departure location of each flight. It can be observed in this figure that the temporal variability is very low in all the flights. In particular, in Flight 1 and Flight 3, the temporal variability is almost negligible during the whole flight time, whereas, in Flight 2, it starts increasing after the first splitting location. However, despite this increase, it is very low in Flight 2 as well, leading to the conclusion that the temporal variability of all the flights slightly depends on the random variable θ.

Fig. 8.4. Experiment A: Expected values of the timing of the optimal trajectories of each aircraft together with the corresponding 95% envelopes.

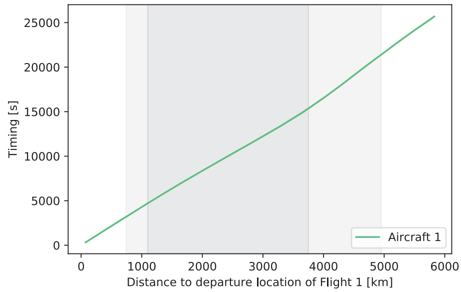

(a) Flight 1

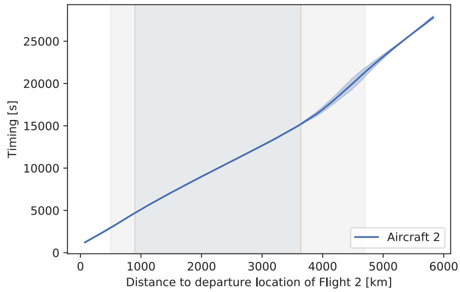

(b) Flight 2

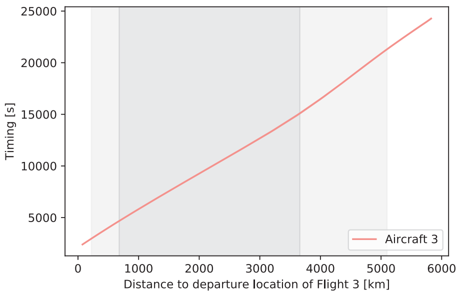

(c) Flight 3

It can be observed in Table 8.2, in which the expected values and the 95% confidence intervals of the rendezvous and splitting times are reported, that the amplitudes of these intervals are lower for the rendezvous times than for the splitting times, but remains fairly small for both of them.

Table 8.2. Experiment A: Expected values and 95% confidence intervals of the rendezvous and splitting times.

	Expected value	95% confidence interval
First rendezvous time [h]	0.88	[0.87, 0.89]
Second rendezvous time [h]	1.32	[1.32, 1.32]
First splitting time [h]	4.19	[4.17, 4.21]
Second splitting time [h]	5.95	[5.92, 5.98]

Direct operating costs

The expected values and the 95% confidence intervals for both the flight time, expressed in hours, and the fuel burn, expressed in tonnes, for each flight are listed in Table 8.3. From the amplitudes of the 95% confidence intervals, it is easy to see that, as already mentioned, the flight time variability is rather low. In contrast, as expected, the uncertainty in the fuel burn savings has a significant impact on the variability of the fuel consumption.

Table 8.3. Experiment A: Expected values and 95% confidence intervals of flight times and fuel consumption of each flight.

	Flight time [h]		Fuel burn [t]	
	Expected value	95% confidence interval	Expected value	95% confidence interval
Flight 1	7.13	[7.12, 7.15]	42.47	[41.19, 43.74]
Flight 2	7.47	[7.43, 7.52]	46.24	[45.90, 46.58]
Flight 3	6.16	[6.15, 6.18]	38.00	[36.58, 39.42]

Comparison with the results obtained in solo flight

To quantify the benefits of formation flight with respect to solo flight, the expected values of the flight time and the fuel consumption, along with the expected value of the corresponding DOC expressed in monetary units, *mu*, are estimated assuming that the three flights are performed as solo flights. The obtained results are reported in Table 8.4. For the sake of comparison, the expected values of the DOC obtained in both formation and solo flights of the three aircraft are reported in Table 8.5. It is remarkable that, in spite of the uncertainties considered in the fuel burn savings for the trailing aircraft, the reduction in the total DOC achieved with formation flight amounts to 2.16%.

Table 8.4. Experiment A: Expected values of flight times, fuel consumption, and DOC in solo flight of the three aircraft.

	Flight time [*h*]	Fuel burn [*t*]	DOC [*mu*]
Flight 1	7.06	45.73	39635.79
Flight 2	7.32	45.44	39713.60
Flight 3	6.02	39.52	34165.60

Table 8.5. Experiment A: Expected values of the DOC in solo and formation flights of the three aircraft.

	Flight 1	Flight 2	Flight 3	Total
DOC solo flight [*mu*]	39635.79	39713.60	34165.60	113514.99
DOC formation flight [*mu*]	37429.40	40435.59	33252.80	111117.79
ΔDOC [%]	−5.89	+1.79	−2.75	−2.16

Comparison with the results obtained in deterministic formation mission design

To quantify the effects of the uncertainty in the fuel burn savings for the trailing aircraft on the DOC, the same formation mission is designed in the absence of uncertainty, in which the fuel burn savings for both the trailing and intermediate aircraft are set to 10%. For the sake of comparison, the obtained results in terms of the DOC for the deterministic and stochastic formation missions are summarized in Table 8.6. It can be seen that the increment of the total DOC due to the presence of uncertainties amounts to 1.60%.

Table 8.6. Experiment A: Values of the DOC in deterministic and stochastic formation missions of the three aircraft.

	Flight 1	Flight 2	Flight 3	Total
Deterministic DOC [*mu*]	36178.9	40205.67	32980.96	109365.53
Stochastic DOC [*mu*] (expected value)	37429.40	40435.59	33252.80	111117.79
ΔDOC [%]	+3.45	+0.57	+0.82	+1.60

8.3. Experiment B: Two-aircraft transoceanic mission design with uncertainty in the departure times of the flights

8.3.1. Description of the experiment

Experiment B involves two transoceanic eastbound flights, Flight 1 and Flight 2, with uncertainty in the departure times of the flights. The flights considered in this experiment have the same departure and arrival locations and the same boundary values for the state variables as Flight 1 and Flight 2 in Experiment A. They have the following departure and arrival locations:

- Flight 1: New York (JFK) - Paris (CDG).
- Flight 2: Boston (BOS) - Madrid (MAD).

The departure times of Flight 1 and Flight 2 are set to 10:15 and 10:30, respectively. The boundary conditions for the state variables of the two aircraft are given in Table 8.1. Flight 1 and Flight 2 are operated by Aircraft 1 and Aircraft 2, respectively.

As in Experiment A, the formation configuration is selected in advance. In case of formation flight, Aircraft 1 will be the trailing aircraft and Aircraft 2 the leader. In this experiment, the fuel burn savings for the trailing aircraft are set to 10%.

The random variables that represent the delays with respect to the scheduled departure times of Flight 1 and Flight 2 from JFK and BOS airports are denoted by θ_1 and θ_2, respectively. These random variables have been modeled using a Gaussian mixture distribution, the parameters of which are estimated from real delay data obtained from the Transtats online database of the U.S. Bureau of Transportation Statistics. This database provides detailed information on the U.S. transportation systems, including data on departure delays by airport and airline. The expectation-maximization algorithm for fitting mixture-of-Gaussian models to data is employed for this purpose [Murphy, 2012]. Departure delay data corresponding to April 2019 are used.

The resulting Gaussian mixture probability density functions that model the random variables θ_1 and θ_2 that represent the departure delays at JFK and BOS airports both have 4 components. The values of the parameters of the Gaussian mixture probability density functions are given in Table 8.7, where $p_{i,j}$, i = 1, 2 , j = 1, 2, 3, 4 are the weights of the Gaussian component probability density functions of θ_i, which are probabilities that sum to 1, and $\mu_{i,j}$ and $\sigma_{i,j}$ are their means and standard deviations, respectively. This result is consistent with previous studies on estimation of flight departure delay distributions [Tu et al., 2008]. Fig. 8.5 shows in black the obtained Gaussian mixture distribution of the departure delays of Flight 1 and Flight 2 from JFK and BOS airports, respectively, together with the histogram of the data. A bin width of 2 minutes is used for the histograms. The components of the Gaussian mixture distribution are represented by dotted lines. The mean and the standard deviation of the random variable θ_1 are −1.67 min and 7.69 min, respectively. The mean and the standard deviation of the random variable θ_2 are −0.88 min and 10.37 min, respectively.

Table 8.7. Experiment B: Estimated parameters of the Gaussian mixture probability density functions that model the departure delays of the flights.

	Departure airport	Random variable	$P_{i,1}, P_{i,2}, P_{i,3}, P_{i,4}$	$\mu_{i,1}, \mu_{i,2}, \mu_{i,3}, \mu_{i,4}$	$\sigma_{i,1}, \sigma_{i,2}, \sigma_{i,3}, \sigma_{i,4}$
Flight 1	JFK	θ_1	0.39, 0.17, 0.27, 0.17	−4.94, 11.94, −0.99, −8.91	2.20, 7.17, 2.93, 2.89
Flight 2	BOS	θ_2	0.24, 0.56, 0.06, 0.14	−1.76, −6.61, 28.67, 10.92	3.39, 3.70, 5.68, 5.78

As in Experiment A, solving this problem entails deciding which mode of flight is optimal, the expected values and standard deviations of the latitude and longitude of the optimal trajectories of each aircraft as functions of time, and the expected values and standard deviation of the timing of the trajectory as functions of the distance.

8.3.2. Results

The sequence of discrete states obtained in the solution is the following:

- State 1: Both aircraft fly solo.
- State 2: The aircraft fly in formation.
- State 3: Both aircraft fly solo.

[1] https://www.transtats.bts.gov/

Fig. 8.5. Experiment B: Estimated probability density functions of the random variables θ_1 and θ_2 that represent the departure delays of each flight.

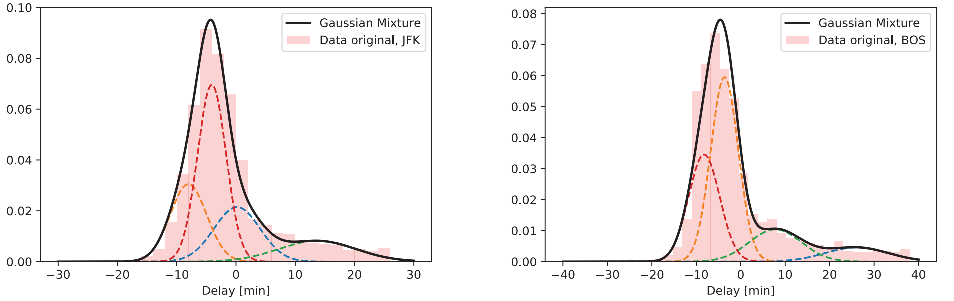

(a) θ_2, departure delay of Flight 1, JFK airport **(b)** θ_2, departure delay of Flight 2, BOS airport

Fig. 8.6. Experiment B: Expected values of the longitude and latitude of the optimal trajectories of each aircraft together with the corresponding 95% confidence envelopes represented on the relevant map together with the wind field.

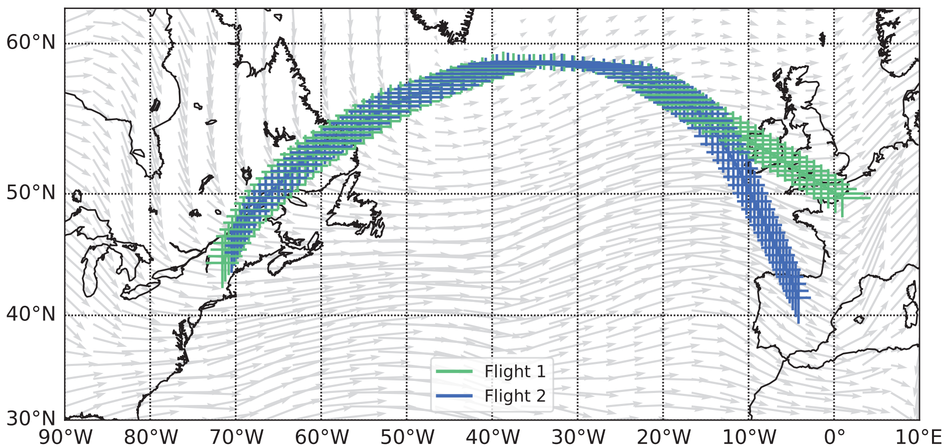

Optimal routes

The expected values of the longitude and latitude of the optimal routes obtained in the solution together with the corresponding 95% confidence envelopes are represented on the relevant map together with the wind field in Fig. 8.6 and as functions of time in Fig. 8.7.(a).

Optimal state and control variables

The expected values of the rest of the state variables, namely, the mass, the heading angle, and the Mach number, together with the corresponding 95%

confidence envelopes are represented as functions of time in Fig. 8.7.(c), Fig. 8.7.(d), and Fig. 8.7.(e), respectively. The expected values of the control variables are represented for the two flights in Fig. 8.8. Green and blue lines correspond to Flight 1 and Flight 2, respectively. As in Experiment A, the portions of the plots of the variables that correspond to State 2, in which the aircraft fly in formation, are represented on a gray background.

It is important to note that all the optimal solutions obtained considering the fuel burn savings that correspond to the nodes of the gPC expansion of the two random variables are formation missions with the same structure.

The control variables vary in a quite smooth way. Comparing the expected values of the state variables and the corresponding 95% confidence envelopes represented as functions of time in Fig. 8.7 with the corresponding ones of Experiment A given in Fig. 8.2, the high variability in every state variable of each flight is striking. In particular, the Mach number variability in the early part of the flight is especially worthy of note. This is due to the fact that anticipations and delays in the departure times of the flights are compensated by increments and reductions of their velocities.

Optimal rendezvous and splitting times

The expected values of the rendezvous and splitting times are reported in Table 8.8 together with the corresponding 95% confidence intervals. State 2, in which the aircraft fly in formation, has the longest duration.

Spatial variability

Regarding the spatial variability of the solution, it can be observed in Fig. 8.6, Fig. 8.7.(a), and Fig. 8.7.(b) that the longitude variability is greater in State 2, in which the aircraft fly in formation. In contrast, the latitude variability has a minimum in State 2, which is located around the maximum value of this geographical coordinate. Aircraft 2, the leading aircraft, has the greatest spatial variability.

Temporal variability

As in Experiment A, in addition to the spatial variability, the temporal variability is also quantified in order to have complete information regarding the spatio-temporal variability of the solution. The expected values of the timing of the solution together with the corresponding 95% confidence envelopes are represented in Fig. 8.9, as functions of the orthodromic distance from the departure locations of each flight. It can be observed in this figure that the temporal variability has a similar behavior for both flights, remaining nearly constant throughout the flight. As in the case of spatial variability, the temporal variability of the flights in Experiment B is considerably greater than the temporal variability of the flights in Experiment A. As expected, uncertainty in the departure times of the flights has a significant impact on the temporal variability of the trajectories, more than the uncertainty in the fuel burn savings for the trailing aircraft.

Fig. 8.7. Experiment B: Expected values of the state variables of the optimal trajectories of each aircraft together with the corresponding 95% confidence envelopes.

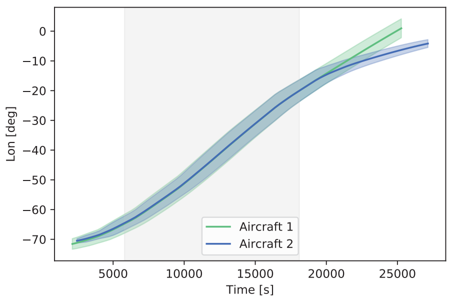

(a) Longitude

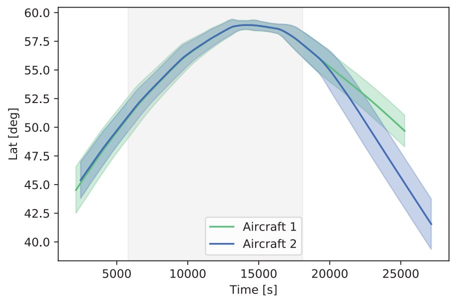

(b) Latitude

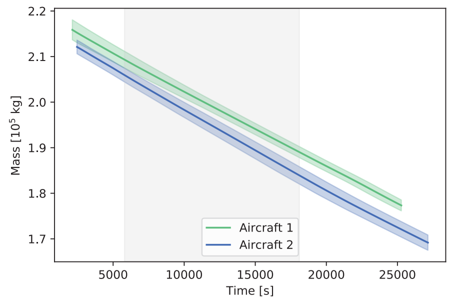

(c) Mass

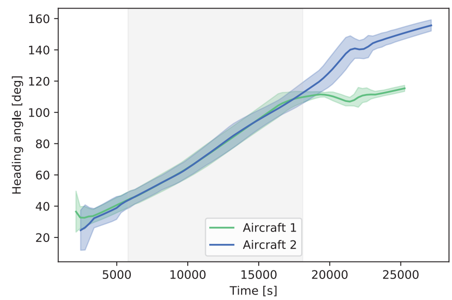

(d) Heading angle

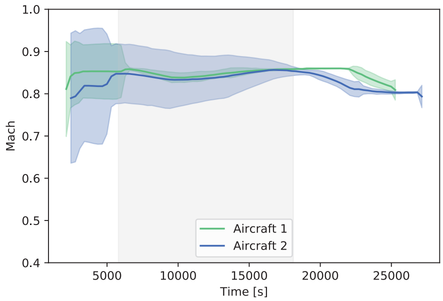

(e) Mach number

Fig. 8.8. Experiment B: Expected values of the control variables of each aircraft.

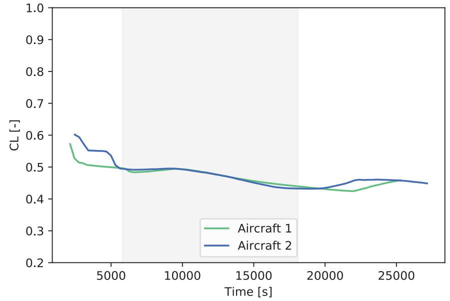

(a) Lift coefficient

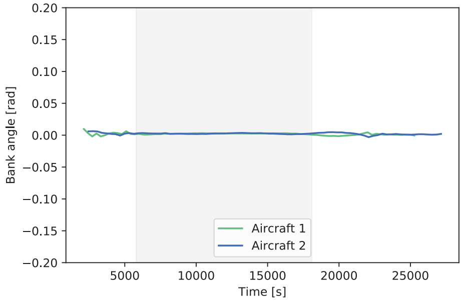

(b) Bank angle

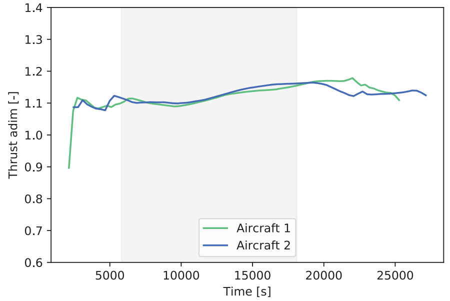

(c) Adimensional thrust

Fig. 8.9. Experiment B: Expected values of the timing of the optimal trajectories of each aircraft together with the corresponding 95% envelopes.

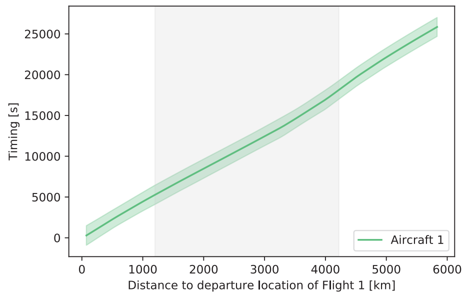

(a) Flight 1

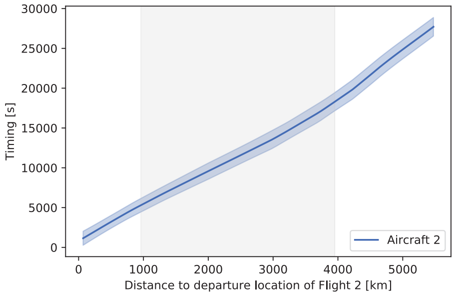

(b) Flight 2

It can be observed in Table 8.8, in which the expected values and the 95% confidence intervals of the rendezvous and splitting times are reported, that the amplitudes of these intervals are similar for the rendezvous and splitting times, being, in both cases, considerably greater than the amplitudes of the 95% confidence intervals of the rendezvous and splitting times obtained in Experiment A.

Direct operating costs

The expected values and the 95% confidence intervals for both the flight time, expressed in hours, and the fuel burn, expressed in tonnes, for each flight are listed in Table 8.9. From the amplitudes of the 95% confidence intervals, it is easy to see that, as already mentioned, the flight time variability is rather high. Additionally, the uncertainty in the departure times also has a significant impact on the variability of the fuel consumption.

Table 8.8. Experiment B: Expected values and 95% confidence intervals of the rendezvous and splitting times.

	Expected value	95% confidence interval
Rendezvous time [h]	1.61	[1.29, 1.94]
Splitting time [h]	5.03	[4.71, 5.34]

Table 8.9. Experiment B: Expected values and 95% confidence intervals of flight times and fuel consumption of each flight.

	Flight time [*h*]		Fuel burn [*t*]	
	Expected value	95% confidence interval	Expected value	95% confidence interval
Flight 1	7.18	[6.86, 7.50]	43.58	[42.52, 44.63]
Flight 2	7.70	[7.37, 8.02]	46.69	[46.27, 47.11]

Comparison with the results obtained in solo flight

To quantify the benefits of formation flight with respect to solo flight, the expected values of the flight time and the fuel consumption along with the expected value of the corresponding DOC expressed in monetary units, *mu*, for the two solo flights, given in the first two rows of Table 8.4, are compared to the expected values of the DOC obtained in formation flight. The obtained results are reported in Table 8.10. It can be observed that, in the presence of uncertainties regarding the departure times of the flights, the probability density funcion of which is estimated from real departure delay data, small benefits are expected in terms of the reduction of the total DOC, which amount to only 0.11%. However, in real-life scenarios, some mitigation measures could be implemented to reduce the negative impact of flight delays on the benefits of formation flight such as adjusting the flight plan of the formation mission before departure when one of the flights of a formation is delayed.

Table 8.10. Experiment B: Expected values of the DOC in solo and formation flights of the two aircraft.

	Flight 1	Flight 2	Total
DOC solo flight [*mu*]	39635.79	39713.60	79349.39
DOC formation flight [*mu*]	38260.39	40999.01	79259.39
△DOC [%]	−3.59	+3.14%	−0.11

Comparison with the results obtained in deterministic formation missions

To quantify the effects of the uncertainty in the departure delays on the DOC, the same formation mission is designed in the absence of uncertainty, in which no delays are considered. For the sake of comparison, the obtained results in terms of the DOC for the deterministic and stochastic formation missions are summarized in Table 8.11. It can be seen that the increment of the total DOC due to the presence of uncertainties amounts to 3.76%.

Table 8.11. Experiment B: Values of the DOC in deterministic and stochastic formation missions of the two aircraft.

	Flight 1	Flight 2	Total
Deterministic DOC [*mu*]	36178.90	40205.67	76384.57
Stochastic DOC [*mu*] (expected value)	38260.39	40999.01	79259.39
△ DOC [%]	+5.75	+1.97	+3.76

Based on the results of the two experiments, it is possible to conclude that uncertainties have a significant impact on the formation flight benefits in terms of the reduction of the DOC. In particular, the uncertainties regarding the departure times have a far greater impact on the DOC than the uncertainties regarding the fuel burn savings. These results demonstrate that formation flight is economically beneficial in the presence of uncertainties regarding the fuel savings for the trailing aircraft and in the departure times of the aircraft.

In the next section, a sensitivity analysis of the solution of this experiment to the random variables that represent the departure times of the flights is carried out. The purpose of this analysis is to quantify how much uncertainty in each component of the solution is due to the different sources of uncertainty considered in the experiment.

8.3.3. Sensitivity analysis

In this section, following Section 6.3, a variance-based sensitivity analysis of the results obtained in Experiment B is conducted through the computation of the Sobol' indices. The aim of this variance-based sensitivity analysis is to quantify what proportion of the variance of the latitude and the longitude of flight k of the solution of the formation mission design problem, $\lambda_k(t, \theta)$ and $\phi_k(t, \theta)$, respectively, is due to the variance of each departure delays of Flight 1 and Flight 2, θ_1 and θ_2, respectively.

The analysis of the sensitivity of the components of the solution obtained in Experiment

Fig. 8.10. Experiment B: Sobol' indices of the geographical coordinates of the optimal trajectories of each flight. Gray and black lines correspond to the random variables θ_1 and θ_2, respectively.

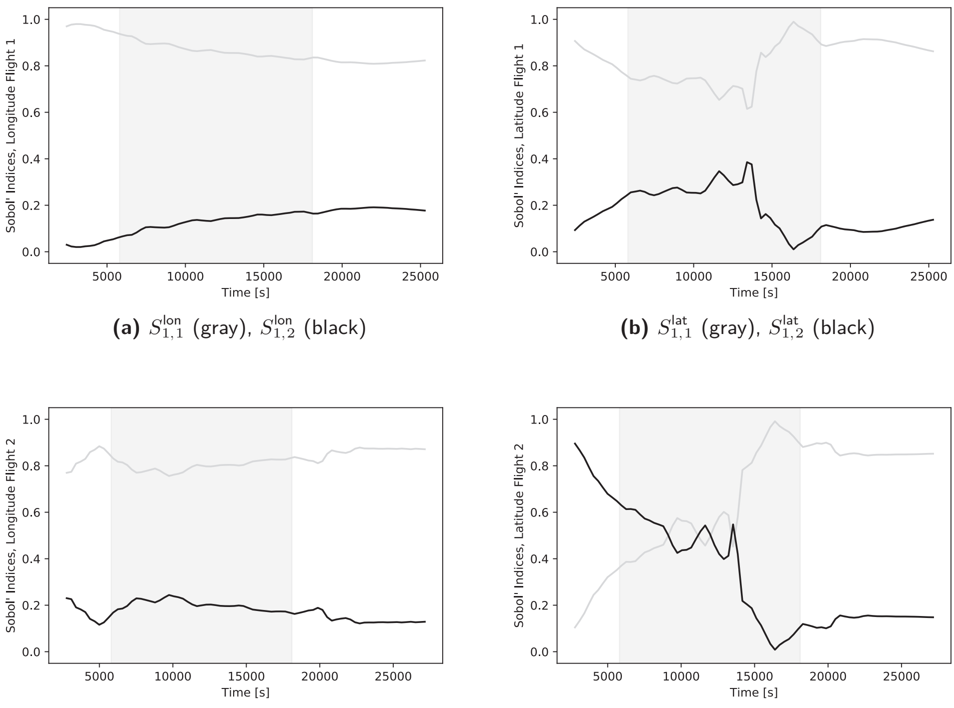

(a) $S^{\text{lon}}_{1,1}$ (gray), $S^{\text{lon}}_{1,2}$ (black)

(b) $S^{\text{lat}}_{1,1}$ (gray), $S^{\text{lat}}_{1,2}$ (black)

(c) $S^{\text{lon}}_{2,1}$ (gray), $S^{\text{lon}}_{2,2}$ (black)

(d) $S^{\text{lat}}_{2,1}$ (gray), $S^{\text{lat}}_{2,2}$ (black)

B to the two random variables θ_1 and θ_2 that represent the departure delays of Flight 1 and Flight 2, respectively, is carried out employing this approach. The Sobol' indices of the latitude and longitude of Flight k, k = 1,2 with respect to the random variable θ_j,j = 1,2 are denoted by $S^{\text{lat}}_{k,j}$ and $S^{\text{lon}}_{k,j}$, respectively. They represent the proportions of the variance of the geographical coordinates of the optimal route of Flight *k* that is due to the variance of the departure time of Flight *j*. The Sobol' indices of the longitude and latitude of the optimal routes obtained in the solution of Experiment B are represented as functions of time in Fig. 8.10, in which Sobol' indices associated with θ_1 and θ_2 are plotted in gray and black, respectively.

It can be seen in Fig. 8.10.(a) and Fig. 8.10.(b) that during the whole flight, most of the variance of both geographical coordinates of the optimal route of Flight 1 is due to the variance of the random variable θ_1. In particular, the percentage of the variance of the longitude of Flight 1 due to the variance of θ_1 is around 90%, while the percentage of the variance of the latitude of Flight 1 due to the variance of the same random variable is between 60% and 90% during the whole flight time.

It can be seen in Fig. 8.10.(c) and Fig. 8.10.(d) that during the whole flight, most of the variance of the longitude of the optimal route of Flight 2 is due to the variance of the random variable θ_1. In contrast, the relative influence of the variance of the random variables θ_1 and θ_2 on the variance of the latitude of the optimal route of Flight 2 changes along the flight. In particular, in the first part of Flight 2, up to 8000 seconds, approximately, the variance of the random variable θ_2 has the most influence on the variance of the latitude of Flight 2. After that, there is an intermediate part of Flight 2, between 8000 and 14000 seconds, approximately, in which the variances of θ_1 and θ_2 have a similar influence on the variance of the latitude of Flight 2. Finally, in the last part of Flight 2, the influence of the variance of θ_1 on the variance of the latitude of Flight 2 becomes predominant, reaching a percentage of 90%.

Fig. 8.11. Experiment B: Sobol' indices of the timing of the optimal trajectories of each flight. Gray and black lines correspond to the random variables θ_1 and θ_2, respectively.

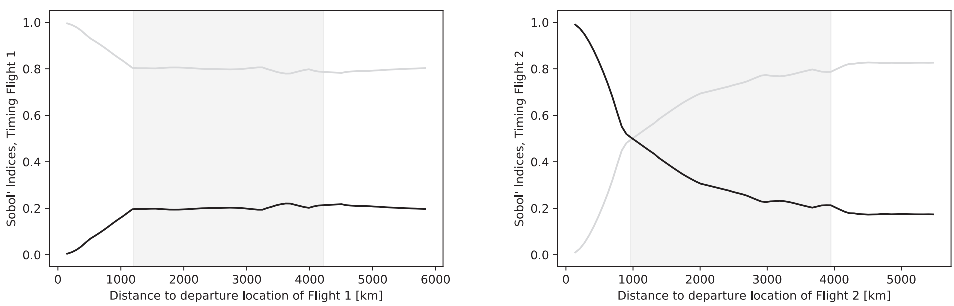

(a) $S^{\text{timing}}_{1,1}$ (gray), $S^{\text{timing}}_{1,2}$ (black), Flight 1

(b) $S^{\text{timing}}_{2,1}$ (gray), $S^{\text{timing}}_{2,2}$ (black), Flight 2

The Sobol' indices of the timing of Flight $k, k = 1,2$ with respect to the random variable $\theta_j, j = 1,2$ are denoted by $S^{\text{timing}}_{k,j}(d_k)$, where d_k is the orthodromic distance of flight k from the departure location. They numerically quantify the proportion of the variance of the timing of the optimal route of flight k that is due to the variance of θ_j. The Sobol' indices of the timing of the optimal routes obtained in the solution of Experiment B are represented as functions of the orthodromic distance in Fig. 8.11, in which Sobol' indices associated with θ_1 and θ_2 are plotted in gray and black, respectively. It can be seen in this figure that, during the whole flight, most of the variance of the timing of the optimal route of Flight 1 is due to the variance of the random variable θ_1, with a percentage of about 80%. On the contrary, the relative influence of the variance of the random variables θ_1 and θ_2 on the variance of the timing of the optimal route of Flight 2 changes along the flight. In particular, in the first part of Flight 2, up to the distance of 1000 km, approximately, the variance of θ_2 has the most influence on the variance of the timing of the optimal route of Flight 2. After that, the influence of the variance of θ_1 on the variance of the timing of the optimal route of Flight 2 becomes predominant, reaching a percentage of 80%.

8.4. Conclusions

The results of the numerical experiments described in this chapter show that uncertainties have a significant impact on the potential benefits of a formation mission. In particular, the uncertainties regarding the departure times have a greater impact on the direct operating costs than the uncertainties regarding the fuel burn savings. The results reveal that the increment of the direct operating costs due to the presence of uncertainties amounts to 1.60% and 3.76% in Experiment A and Experiment B, respectively. However, even in the presence of uncertainties, reductions of the direct operating costs are expected with formation flight compared to solo flight in both experiments. The results also give interesting additional information, revealing, for instance, that one random variable may have predominant influence on the variability of a component of the solution. They also indicate that the relative influence of the random variables on the variability of a component of the solution may change during the flight. The results of the numerical experiments described in this chapter show that the proposed methodology is an effective tool for solving the formation mission design problem for commercial aircraft in the presence of uncertainties.